PCCP

PAPER

Check for updates

Cite this: Phys. Chem. Chem. Phys., 2017, 19, 19010

Two-layer and composite films based on oxidized and fluorinated graphene

A. I. Ivanov, *[a] N. A. Nebogatikova, *[a] I. A. Kotin [a] and I. V. Antonova [abc]

This study is devoted to the production and investigation of dielectric films, based on oxidized and fluorinated graphene suspensions. The properties of the graphene oxide films may be greatly improved by adding fluorographene. FG films have transmission in the visible and near infrared ranges equal to 96–98%. Two-layer films of fluorinated graphene on graphene oxide and composite films (composite suspension of fluorinated and oxidized graphene) exhibit good insulating properties. Their leakage currents are lower than that in the graphene oxide or fluorinated graphene by 3–5 orders of magnitude. A significant increase in thermal stability and relatively low charge in the film and at the interface with silicon (3×10^{10}–1.4×10^{11} cm^{-2}) are also found for these films. An application of thin fluorographene films (a few nanometers) decorates and eliminates structural defects in the graphene oxide films, resulting in conductivity blocking in graphene oxide. The built-in charge density in the composite film of 10–20% fluorographene in the graphene oxide is much less than in the two-layer film ($<1 \times 10^{10}$ cm^{-2}). The created two-layer and composite films may be practically applied in 2D printed and flexible electronics as insulating films (gate dielectric and interlayer insulator), as well as materials showing the resistive effect.

Received 29th May 2017,
Accepted 22nd June 2017

DOI: 10.1039/c7cp03609d

rsc.li/pccp

1. Introduction

Graphene based 2D printed and flexible electronics is a recently emerged and fast growing field that has attracted large scientific and technological interest in the past few years.[1,2] These techniques can pattern special materials (liquid composites) on either rigid or flexible substrates, at low temperature and over large areas, and most importantly at very low cost. However, the performance of printed devices is limited by the quality of the materials, contained in the inks, and the arrangement of these materials on the target substrate. Organic materials, as a rule, have significantly limited stability, reliability and durability of the resulting devices.[3,4] Graphene and other two-dimensional (2D) materials may be a solution of these problems due to very promising physical and chemical properties even in the form of liquid compositions.[5–9] The appearance of new graphene based materials and expansion of possible applications of 2D printed materials for modern electronics and photonics are expected in the near future.

Nowadays, there is constant progress in the use of solution-processed or printable electronic components for developing flexible, smart, cheap, disposable and large area biosensor arrays, drug-delivery electronic patches, implantable devices, super capacitors, thin film batteries, *etc.*[10–13] Printable thin-film transistors (TFTs) have evolved to high-performing sensors and other wide spectrum applications. The conductive graphene films or reduced graphene oxide layers are considered as materials for TFT channels or electrodes. Dielectric materials play a critical role since the carrier transport takes place at the interface between the dielectric and the semiconductor; therefore the quality of such an interface determines the device performance. For instance, this fact was experimentally demonstrated by S. Lim[14] when the use of the inkjet-patterned RGO/PVA electrodes increased field-effect mobility of the bottom-contact pentacene TFTs to 0.23 cm^2 (V s)$^{-1}$, which was significantly enhanced relative to that of TFTs with Au or PEDOT:PSS electrodes. Nowadays, dielectric layers for graphene heterostructures and field effect transistors are usually made of materials such as h-BN, Al_2O_3, and HfO_x. We have proposed the dielectric films based on graphene derivatives for printed and flexible graphene electronics.

Recently, we have developed a new approach to create a fluorinated graphene (FG) suspension.[15–17] The peculiarity of this suspension is that the lateral size of the FG flakes was ~10–100 nm with a thickness of 0.4–2 nm. It is worth emphasizing that in spite of a relatively low fluorination degree (F/C ~ 25%) our films demonstrate a transition into the insulated state, complete vanishing of lines in the Raman spectra and the high transparency of suspension and films in the light in visible and near infrared ranges. One of the key parameters of the thin FG films is the ultra-low built-in charge with an

---

[a] *Rzhanov Institute of Semiconductor Physics SB RAS, Acad. Lavrentiev Avenue 13, Novosibirsk 630090, Russia. E-mail: aiivanov@isp.nsc.ru, nadonebo@gmail.com*
[b] *Novosibirsk State University, 630090, Pirogov Street 6, Novosibirsk, Russia*
[c] *Novosibirsk State Technical University, 630073, K. Marx Avenue 20, Novosibirsk, Russia*

approximate 10^{10} cm^{-2} density in the films and at interface traps with different semiconductors and good insulating properties in the case of a relatively high fluorination degree. Huge perspectives of FG functional layers are envisaged. This study analyzes and compares the properties of dielectric layers of fluorinated graphene, layers from composite suspension GO–FG, graphene oxide (GO) suspension and two-layer FG/GO films in metal–insulator–semiconductor (MIS) heterostructures, created by means of printed technologies.

2. Experimental

2.1. Sample preparation

The materials used in this work were created on the basis of the graphene compounds: graphene oxide and fluorinated graphene. Graphene oxide was obtained using a modified method of Hummers.[18] The characteristic thickness of the GO flakes in the suspension was 0.5–1.5 nm, and lateral dimensions ranged from 100 to 400 nm. The typical lateral size of the FG flakes was ∼10–20 nm with a small number of relatively large flakes (up to 100 nm). The thickness of the FG flakes was 0.4–2 nm.

Fluorination of the graphene suspension was performed by means of the treatment of the graphene suspension in an aqueous solution of hydrofluoric acid.[15,16] The evidence of fluorination is based on the reversible transition from the insulating to the conductive state, the high temperature stability (up to 450 °C with a fluorination activation energy of 2.0 eV), the vanishing of all peaks in the Raman spectra, a dielectric constant value of 1.2 for the fluorinated films created from the suspension, and the transparency of the fluorographene suspension.[16,19,20] These properties correspond to fluorinated graphene in contrast to graphene oxide.

The film structures were created from a single-component and composite suspensions. Graphene oxide and fluorinated graphene films were obtained by suspension application on the substrate surfaces. Two-layer structures were fabricated by suspension application stepwise on a substrate after full drying of the first layer. Designation of the structures and their brief description are presented in Table 1.

We used two methods to create films: suspension application to a substrate using drops and 2D printing. As is schematically shown in Fig. 1, the first step consists in treating the surface where films are to be deposited. Depending on the material of the first layer structure, the surface is treated with various substances to improve wetting and adhesion. According to our observations, the graphene oxide and fluorinated graphene water-based suspensions have a good spreading on the silicon surface. The reason for this observation is the fact that the surface tension of suspensions is low enough for spreading. Suspensions contain the traces of various acids and other chemical substances used for their preparation. Moreover, the surface with a native oxide is hydrophilic. A scanning electron microscopic (SEM) image of the treated silicon surface is shown in Fig. 1b. The second step is the application of the required film or the first layer structure. Fig. 1d and e show schematic images of structures with one and two layers of the deposited suspension using droplets or 2D printing. For the case when a structure is created by droplet deposition Fig. 1f and g show SEM images of the graphene oxide film surface on the silicon substrate and the fluorinated graphene film surface on GO/Si, respectively. The second layer of fluorinated graphene was deposited only after complete drying of the first one. In the case of SiO_2/Si substrates, films of polyvinyl alcohol (PVA) were used. PVA is a synthetic water-soluble polymer with the chemical formula $(C_2H_4O)_n$. We used the PVA powder with a molecular weight of 13 000. The PVA film deposited on the surface of SiO_2/Si provides a good adhesion upon applying water-based suspensions. In addition, PVA is widely used to ensure adhesion of water-based ink when printing on flexible substrates. Therefore, the interaction of PVA with FG and GO layers was of particular interest. The PVA layer was applied using a spin-coater, and the characteristic layer thickness was 20 nm. Fig. 1i shows a schematic step of the synthesis of PVA/SiO_2/Si substrates, and Fig. 1k presents a SEM image of the PVA surface. Schematic and SEM images of the FG film surfaces created by printing on PVA/SiO_2/Si substrates are shown in

Table 1 Created films, method of suspension deposition, and some film parameters: d is the film thickness, ε is the effective permittivity of the films, and Q_F is the fixed charge whose density was negative. Q_F/q_e was extracted from C–V curves with the use of flat-band voltage, where q_e is the electron charge

Sample	Film description	d, nm	ε	Q_F^*/q, cm^{-2}
GO_{drop}	GO film, drops	90–110	4.3	$(0.8–2) \times 10^{11}$
GO_{print}	GO film, printing	30–40		
FG_{drop}	FG film, drops	20–40	1.1	$(0.5–5) \times 10^{10}$
FG_{print}	FG film, printing	2–5		
FG/GO_{drop}	Two-layer films, drops $d_{FG} \sim 30–40$ nm, $d_{GO\text{-}1} \sim 70–90$ nm	110–120	3	$(0.3–2) \times 10^{11}$
FG/GO_{print}	Two-layer films, printing $d_{FG} \sim 2–3$ nm, $d_{GO\text{-}2} \sim 33–37$ nm	35–40		
$GO–FG_{drop}$	Composite film, drops FG ∼ 10–20 wt%	∼80	1.3–1.7	$(0.4–1) \times 10^{10}$
$(GO–FG)/FG_{drop}$	Composite film on FG, drops	80–90	1.4	$(0.6–2) \times 10^{10}$
FG/PVA_{print}	Two-layer films, printing	∼40	—	—

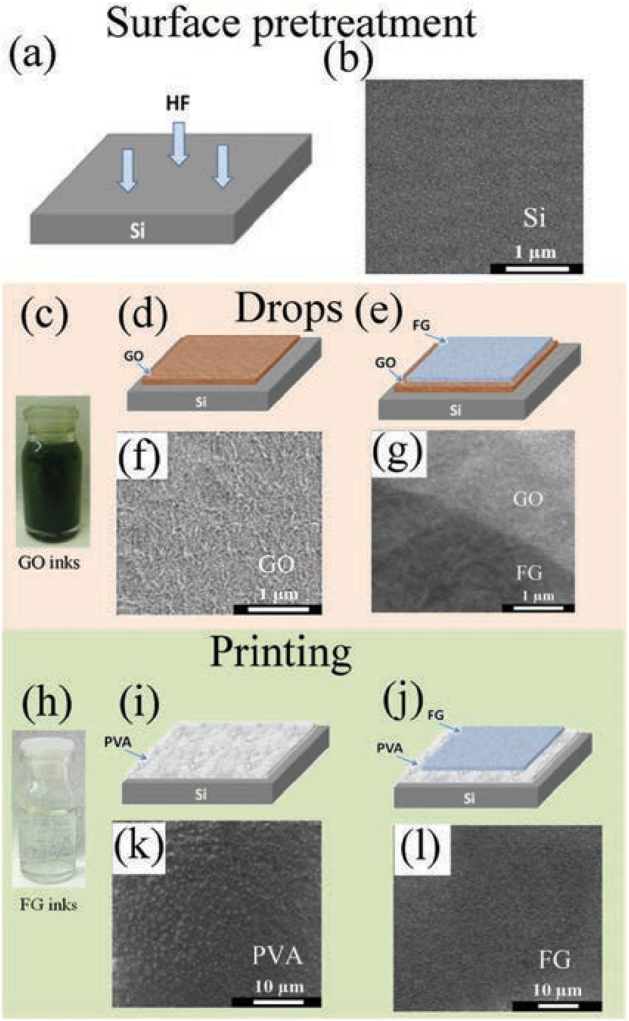

Fig. 1 Steps of the structure synthesis. Stepwise schematic representation of multilayer structures with SEM images of structure surfaces, explaining the process stages. (c and h) images of the various inks. Technological steps are described in the text.

Fig. 1j and l, respectively. Besides, Fig. 1c and h show photos of graphene oxide and fluorinated graphene suspensions.

In the case of film printing, flexible substrates were also used in addition to silicon: (1) polyethylene terephthalate (PET) with an adhesive coating (Lomond inkjet) for printing with water-based ink, (2) PET with a thin film of polyvinyl alcohol (∼20 nm thickness) to improve adhesion, and polyimide (PI) films produced by Kapton company.

For printing with graphene oxide we used an aqueous suspension with a GO concentration of 2 mg ml^{-1}. The thickness of the layer applied in one printing cycle was ∼1.5 nm. Therefore, 20–25 layers were printed to create a film with a thickness of 30–40 nm. When printing with fluorinated graphene a water-based suspension with a FG concentration of ∼0.5 mg ml^{-1} was used, and less than one monolayer was applied for one printing cycle. The maximum film thickness was ∼2–5 nm at printing from 5 to 10 layers. When films were created using drops, the same suspensions as in printing were applied. The drop volume was controlled and amounted to 50 μl. This allowed creating several almost identical structures, where the film thickness varied within 10%. The printer Dimatix FUJIFILM DMP-2831 was used for printing. The printed layers were dried after each printing cycle at a temperature of 60 °C. As a result, there was no mixing of the printed layers.

The electrical contacts to the films were prepared by silver alloy coating onto the film surface, the contact surface area was approximately 0.5 mm^2. In the case of silicon substrates, a set of vertical metal–insulator–semiconductor (MIS) structures for different films was created. These structures were used for vertical measurements of current–voltage or capacitance–voltage characteristics. Measurements of current–voltage characteristics between two neighbor contacts on the film surface were marked as lateral measurements which can be performed for structures on the Si, SiO_2/Si or flexible substrates. In addition, the silicon substrates with evaporated Au layers or Au contacts on SiO_2/Si substrates were used as well. In this case vertical structures of Ag/film/Au/Si and lateral structures with the film deposited on the contacts were obtained.

2.2. Measurement methods

Layer resistance of the films was studied with the use of the four-probe JANDEL equipment and the HM21 Test Unit. For measuring capacitance–voltage (C–V) and current–voltage (I–V) characteristics, an E7–20 immitance meter and a Keithley picoampere meter (model 6485) were used.

A Solver PRO NT-MDT scanning microscope was used for obtaining atomic force microscopy (AFM) images of the film and substrate surfaces and for determining the film thickness. The measurements were performed in both contact and semi-contact mode. Scanning electron microscopy images were obtained using a JEOLJSM-7800F scanning electron microscope with the energy of primary electrons equal to 2 keV. For recording the X-ray photoelectron spectra (XPS), an SSC Riber facility (Surface Science Centre Riber) was used. The measured XPS spectra permitted studying the chemical composition of the obtained films. The film transparency was analyzed using a spectrophotometer SF-56.

3. Experimental results and discussion

3.1. Structure of films based on graphene compounds

Typical X-ray photoemission spectra of the films created from the fluorinated graphene suspensions are presented in Fig. 2. It is worth mentioning that only peaks C-CF (285.6 eV) and CF (288.3 eV) are observed in the XPS spectra near the C1s peak. Generally, in other cases of fluorination, peaks CF_2 and CF_3 are presented in the spectra.[21–23] In our case, these peaks are not observed. The F1s and C–F peak positions corresponded to semiionic bonds.[24] Semiionic bonds F1s and C–F are typical of graphene or GO fluorination in the HF solution[25,26] and are observed in a wide spectrum of other studies. The formation of semiionic bonds can be connected with the formation of H-bonds with F atoms of F–C in the water solution.[24]

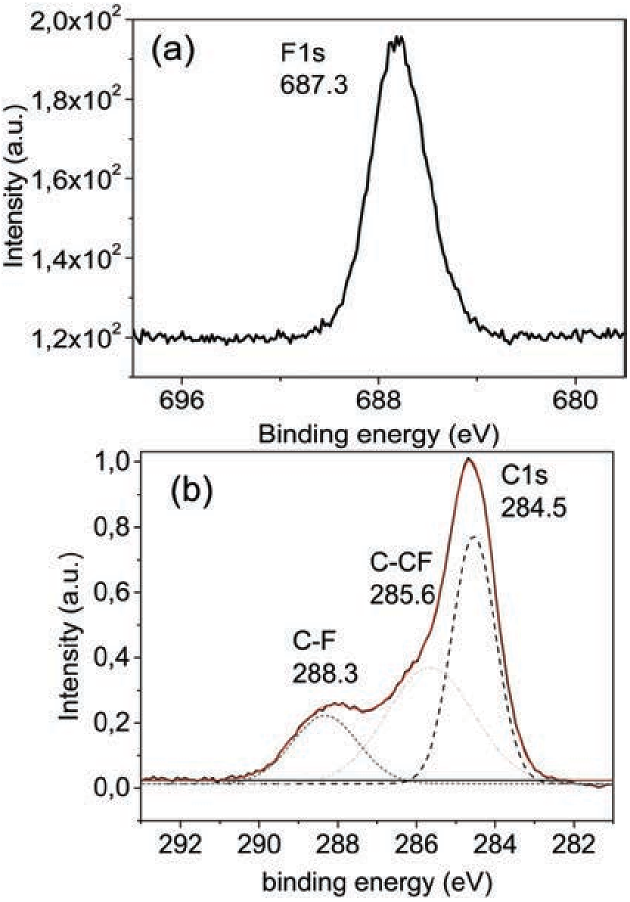

Fig. 2 Study of the fluorinated graphene films using X-ray photoelectron spectroscopy (XPS): (a) part of the spectrum with the F1s peak, and (b) the spectrum near the peak of C1s with decomposition into component lines.

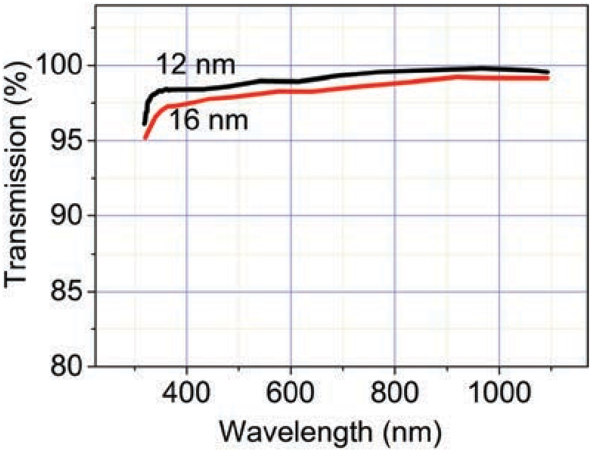

Fig. 3 Transmission of FG films with a thickness of 12 and 16 nm printed on PET substrates in the visible and near infrared ranges.

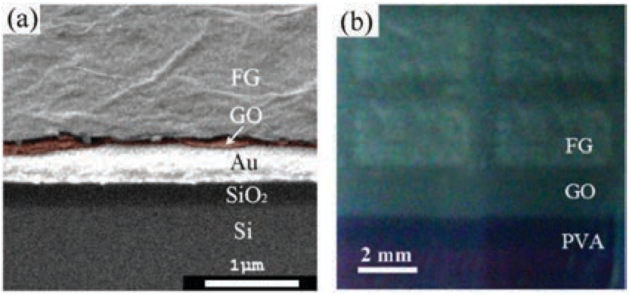

Fig. 4 (a) Cross sectional SEM image of a two-layer structure of FG/GO/Au on SiO$_2$/Si substrates and (b) photograph of the printed structure of FG/GO/PVA/PET with a thickness of different layers from 4 to 30 nm.

The fluorination degree is estimated from the ratio of peak areas F1s to C1s (284.5 eV). It is extracted from the data of Fig. 2 and equals ~19%. The formula $x_{\text{tot}} = S_{\text{C-F}}/(S_{\text{C}} + S_{\text{C-CF}} + S_{\text{C-F}})$, where S is the peak square, was used for the estimation of sample composition CF_x from the results of the C1s peak deconvolution into components. The obtained result is $CF_{0.18}$–$CF_{0.24}$. The average fluorine content in the fluorinated part of flakes can be found as $C_{\text{F}} = S_{\text{C-F}}/(S_{\text{C-CF}} + S_{\text{C-F}})$.[27] This parameter was estimated as $CF_{0.30}$–$CF_{0.35}$. In the average, we suggested, for our samples, the composition formula as C_4F ($CF_{0.25}$). This fluorination degree, as it is demonstrated below, is enough for the formation of insulated FG films.

Fig. 3 presents the transparency spectra obtained for two films with different thicknesses (12 and 16 nm) printed at PET substrates. One can see that the transmission is equal to 96–98% in a wide range of wavelength. It can be considered as an additional argument for strong modification of the graphene suspension properties under a simple treatment in the aqueous solution of HF. The transparency of our fluorinated films in the visible range means that the bandgap is higher than 3 eV.

Let us consider the structure and appearance of the resulting films. Fig. 4a shows the electron microscopy image of the two-layer FG/GO films, deposited with drops on the surface of Au/SiO$_2$/Si. To show the FG/GO interface better, the GO films were colored brown. Fig. 4b shows the photograph of the FG/GO structure printed on the PVA surface.

The AFM image of the printed FG film surface deposited on the Si substrate is presented in Fig. 5a. Since the concentration of fluorographene in this case was small, islands of the fluorinated graphene films were formed, and between them there were individual visible flakes of fluorinated graphene on the surface of silicon. When the FG layer was applied to the GO the islets did not form, but there was a uniform distribution of smaller FG flakes over the surface of larger GO flakes as shown in Fig. 5b. Without FG flakes GO have no corrugation-like relief on their surface. By the example of separate GO flakes one can more clearly see how FG flakes cover their surface. This image also demonstrates the good affinity between GO and FG flakes. In the case of forming a continuous and, accordingly, a thicker FG/GO film it is hard to visualize the FG flakes (Fig. 5c).

However, it may be assumed that the large surface relief (~50 nm) is created by a GO surface, and the lower film of the structure, and the smaller relief (~3–8 nm) is formed by the FG flakes, located on top of the GO. Fig. 5d shows the AFM image of the FG/PVA surface for the structure printed on the SiO$_2$/Si substrate. As a result of partial dissolution of the PVA surface, when printing the fluorographene layer, the FG–PVA composite

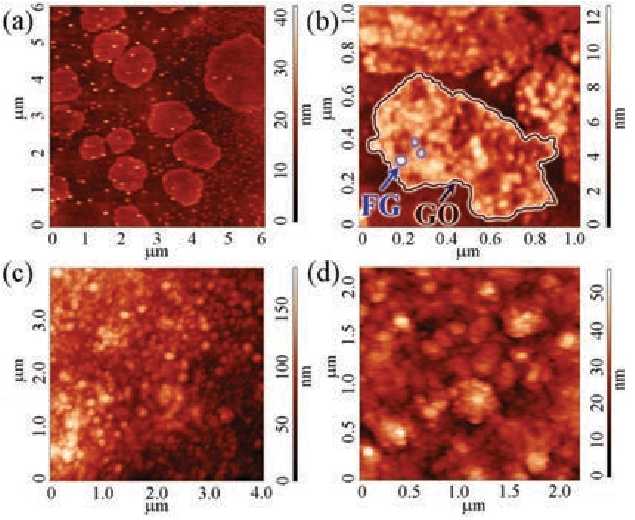

Fig. 5 AFM images of the structure surfaces: (a) image of the forming fluorinated graphene islands, obtained by printing on a silicon surface; between the islands there are visible small fluorinated graphene flakes; (b) image of graphene oxide flakes, whose surface is decorated with fluorographene; (c) image of the continuous graphene oxide film surface, coated with fluorinated graphene flakes: the large-scale relief of the surface ($\sim$50 nm) is created by the GO, and the small relief is formed by FG flakes ($\sim$3–10 nm), located on the surface of GO; (d) an image of the FG–PVA structure printed on the SiO_2 surface.

is obtained. The printed GO layers and films, created by droplets, were discussed in detail in ref. 28. The main conclusion is given in ref. 28 and important for the present study is that the application of a thin film of PVA for hydrophilicity of the substrate ensures the uniform application of ink, a denser film structure, and a lower surface topography. The resulting GO film has a structure similar to the layers created by drops.

The study of the structural properties of the two-layer and composite films on flexible substrates (PET and PI) has shown that fairly dense and smooth films are formed. PVA and other coatings provide good adhesion of the graphene oxide and fluorinated graphene to such substrates, allowing bending layers without changes in the film structure visible by the method of AFM.

Surface roughness of different films on rigid substrates was extracted from AFM images (test area was 2 × 2 μm^2): the surface roughness for GO films was 8.1 nm, for FG/GO films $\sim$5.7 nm, and for FG films $\sim$1.5 nm. The maximal roughness was characteristic of composite GO–FG films (above 10 nm).

3.2. Electrical properties of the two-layer and composite films based on FG and GO

The properties of FG on GO two-layer films were the most extensively studied. Fig. 6a and b show the current–voltage characteristics of FG/GO_{print} two-layer films, created by printing and measured in lateral and vertical configurations. Similar studies of the properties of the $GO–FG_{drop}$ film created by applying drops to the surface of the silicon substrate are demonstrated in Fig. 6c. It has been found out that the magnitude of the

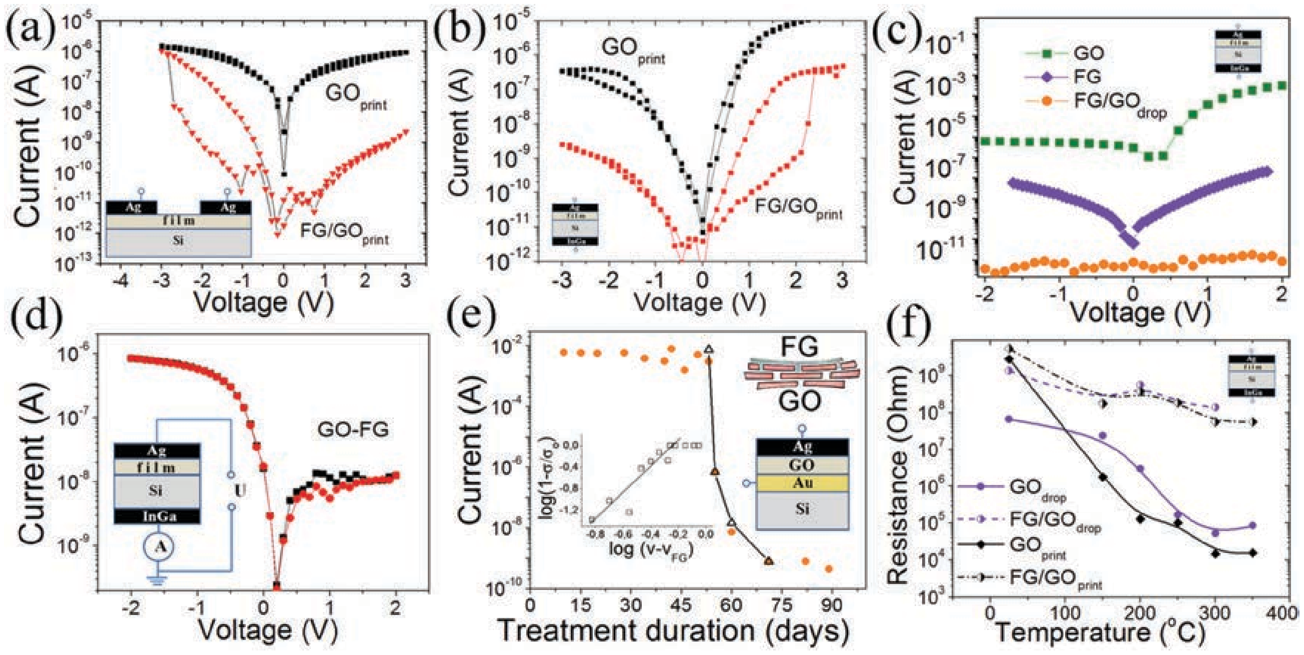

Fig. 6 Current–voltage characteristics of two-layer and composite films (insets give the sketch of used structures): *I–V* curves of the FG/GO_{print} structure of 20 GO layers and 5 FG layers and for GO films before FG printing (a) for lateral and (b) vertical structures; thickness of the printed graphene oxide layers is $\sim$35 nm, and thickness of fluorinated graphene is $\sim$2–3 nm. (c) Comparison of the *I–V* curves through the GO, FG and FG/GO films deposited by droplets. (d) Current–voltage characteristics for the vertical structure of the composite GO–FG films. (e) Dependence of the current through the films with a vertical structure deposited by droplets, depending on the time of graphene fluorination; thickness of the GO–FG films is about 120 nm, and the one of FG films is 25–30 nm. (f) Dependence of the current through the two-layer FG/GO and GO films on the annealing temperature; the considered films were obtained by printing and applying droplets.

current through the two-layer structure is significantly lower than that through the separate films of GO or FG, as shown in Fig. 6c. In both cases, the increase in the two-layer film thickness is not so significant in comparison with the effect of reducing the current through the film by several orders of magnitude, especially in the case of printed layers. For the GO layer with the thickness increasing from ~30 nm to ~80 nm, the leakage current weakly decreases, by about an order of magnitude. As it follows from Fig. 5b, GO and FG flakes demonstrate the good affinity for each other. As mentioned above, the surface roughness of the GO films was 8.1 nm, whereas the surface roughness of the FG/GO films decreased to 5.7 nm for the same area ($2 \times 2\ \mu m^2$). These facts allow suggesting that when applying the fluorinated graphene layer, primarily the ''healing'' of structural defects in the GO films takes place, especially that the lateral size of FG flakes (20–40 nm) is significantly smaller than that of the GO flakes (100–400 nm).

A GO suspension with a smaller flake size was created by means of filtration on the track membrane with pores of 120 nm. Then, two-layer GO (small size)/GO films were formed by drops on Si substrates. The measurements of *I–V* curves demonstrate that the top layer of GO flakes with a small size practically does not change the leakage current through the GO films. Thus, the insulating properties of FG are the most important ones for decreasing the leakage current.

Fig. 6d shows the current–voltage characteristics of a composite GO–FG film. The current–voltage characteristics close to the characteristics of the two-layer FG/GO_{print} are obtained; and the only fact to mention is a large thickness of the GO–FG films compared with FG/GO_{print}. In general, the current at negative voltages does not exceed 1 μA (the regime of silicon surface enrichment with a carrier, when the conductivity is determined only by that of the GO–FG films).

All films obtained by printing were studied using the 4-probe head; and it was found that in all cases the sheet resistance of the films was more than 10^8 Ohm sq^{-1} (the upper limit of sensitivity).

The way the current through the two-layer films is dependent on the time of graphene fluorination in the aqueous solution of hydrofluoric acid is shown in Fig. 6e. The method of producing fluorinated graphene in an aqueous solution of hydrofluoric acid is discussed in detail in ref. 15. The increase in fluorination time increases the degree of graphene fluorination. This figure shows that a high degree of graphene fluorination is required for obtaining insulating layers, and, in the case of fluorination at room temperature, this is achieved in 60 days. The use of higher temperature significantly accelerates the process of fluorination.[15] A sharp transition in the insulating state corresponds to the disappearance of percolation conductivity.

The dependence of film conductivity on the fluorination degree near the threshold of percolation may be described using the well known expression for percolation conductivity:

$$\sigma \sim \left(\nu_{G} - \nu_{G,crit}\right)^{i}, \tag{1}$$

where the conductivity σ is proportional to the number of conductive non-fluorinated paths, ν_G is the portion of the graphene regions in the film, $\nu_{G,crit}$ is the critical volume fraction of graphene, at which the film transition to the insulating state begins, i is the conductivity exponent, controlled by the dimensions, form and orientation of conductive fillers. The value of the parameter $i \sim 3.1$ was determined by modeling the dependence $\log(1 - I/I_o)$ on the duration and degree of fluorination (the inset in Fig. 4e). The value i is close to the value of the parameter $i \sim 2.7$–3.8 obtained in ref. 29–31 at studying the percolation conductivity of the composite materials, based on graphene and carbon nanotubes in the polymer matrix. A large value of the exponent is usually associated with a high aspect ratio of flakes, which is typical for graphene.[32,33]

The parameter of the critical graphene content for percolation conductivity disappearance $\nu_{G,crit}$ was ~0.25 (C_4F compound). It coincides with the data for fluorinated graphene films with 25% content of fluorine that can be good insulators,[19] and with the estimates of the fluorination degree obtained in ref. 16 on the basis of X-ray photoemission spectroscopy measurements. The volume share of the graphene islands (conductive areas of partially fluorinated flakes in the suspension) at which the percolation conductivity disappears, for a three-dimensional film may be written as follows:

$$\nu_{G,crit} = 27\pi d^2 t/4(d + d^*)^3, \tag{2}$$

where d and t are the size and thickness of the non-fluorinated graphene areas, and d^* is the distance between conductive islands (fluorinated edges of the flakes).[34] The critical distance for the electron jump is considered to be 10 nm.[35] The distance between adjacent conductive islands for our films was estimated as $d^* \sim 5$–10 nm at a flake thickness of 1–2 nm and the conductive area size of the flakes was ~50–80 nm. The value of d^* may strongly depend on the shape and orientation of the conductive graphene flakes and their size, as well as on their share in the total film volume. The used ratio well describes thin films consisting of several layers of partially fluorinated graphene flakes.

Assessment of the thermal stability of structures required investigation and comparison of the conductivity of GO and FG/GO films, obtained by applying drops and printing. Fig. 6f shows the dependencies of film resistance on the temperature of isochronous (20 min) annealing, which was carried out in an inert atmosphere (Ar with addition of 10% H_2) at temperatures up to 350 °C. The graphs show that the resistance of the two-layer structures, both printed and created by drops, does not change by more than 1–1.5 orders, while the resistance of the graphene oxide films in both cases varies by 3–5 orders of magnitude. Therefore, the two-layer FG/GO films are much more stable than the GO films, since the application of the second layer greatly suppresses the GO recovery during heating.

To study the properties of two-layer and composite films we used the capacity–voltage characteristics (*C–V*) measured for our MIS structures. From *C–V*, the fixed charge density in the films was determined from flat band voltage (see Table 1). The flat band capacitance CFB was theoretically calculated for an

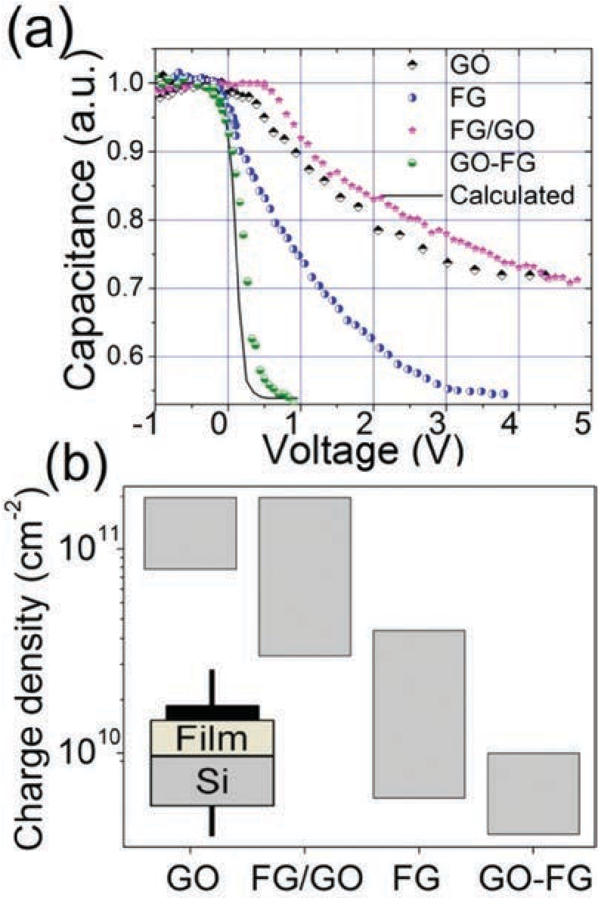

Fig. 7 (a) Capacitance–voltage characteristics of the films of graphene oxide, fluorinated graphene, two-layer films and films obtained from the composite slurry of GO–FG, the ideal *C–V* curve calculated for the structure with charge $Q/q = 0$ cm^{-2} for FG and GO–FG films; (b) charge density in different films considering statistics: GO, two-layer FG/GO, FG and the composite GO–FG for both methods of application.

ideal MIS structure with zero fixed charge. Using this CFB an experimental value of the flat band voltage UFB was extracted from the measured *C–V* characteristics, and then the density of the flat band charge was calculated. Fig. 7a compares the *C–V* characteristics of the main types of films: GO, FG films, the two-layer FG/GO films and the composite GO–FG films. All films were deposited on a silicon substrate, pre-treated with a weak solution of hydrofluoric acid. The data given in Fig. 7b are a summary of the measurements and film parameter calculations for 10–15 structures of each type. The comparison shows that the *C–V* characteristics of the composite films have both the steepest slope and the minimum flat band voltage (*i.e.* the minimum density of interface states and the minimum fixed charge $\leq 10^{10}$ cm^{-2}). The FG/GO two-layer films and GO, accounting for statistics, have the maximum density of the surface states and the maximum fixed charge ($\sim 10^{11}$ cm^{-2}). Thus, the charge density in the composite films is much smaller than in other films, as is shown in Fig. 7b for the fixed charge, determined on the flat band voltage.

The second parameter determined from *C–V* characteristics is the relative dielectric constant ε of the films. The film thickness was measured by AFM, and then from the maximal capacitance value, the relative dielectric constant ε of the films was calculated. The obtained results are shown in Table 1. For GO and FG the values of ε were found (4.3 and 1.1) to well agree with the literature data for these materials.[16,36,37] For two-layer and composite films the obtained values are effective, and for the two-layer films they are well described by the same values of ε taking into account the layer thicknesses.

3.3. The resistive effect in the films based on graphene compounds

Investigation of the electrical properties of the films has revealed the resistance switching in almost all cases. The resistive effect in the films of graphene oxide is described in ref. 38 and 39. Previously the resistive effect was observed by us for the fluorinated graphene films.[17] The resistance switching for different films, found in this study, is presented in Fig. 8; insets in the figures show structures used for measurements. For the lateral and vertical configuration of the structures created on the GO films (Fig. 8a and b) the change in resistance is an order that is sufficient to create a memristor,[39] but the effect is unstable, and after 3–4 switches the *I–V* hysteresis is greatly reduced due to the graphene oxide reduction in the area of the current flow. GO reduction was clearly observed due to a change in the film color (to black) between contacts.

Fluorinated graphene films show a stable but relatively weak resistive effect (3–5 times depending on applied voltage), as demonstrated in Fig. 8c. Similarly, the most stable bipolar resistive effect with a small (3-fold) change in resistance was observed for the two-layer FG/GO films, Fig. 8d. Composite GO–FG structures demonstrated the resistive effect with the change in resistance by 2 orders of magnitude, as shown in Fig. 8e; but it was unstable; and after 2–3 switches the film retained a high resistive state. The strongest and the most stable unipolar resistive effect with one order change in resistance was observed for the FG/PVA films. Current–voltage characteristics of this structure are shown in Fig. 8f. It should be noted that the effect of switching with no change was observed at a voltage of 2.5–3 V for 50 cycles, and the sweep speed was $\sim$4 V min^{-1}. Fig. 6f shows data only for 20 cycles of the measurements; in reality, more than 50 cycles were recruited by periodic measurements on this sample for a month, and no change in the hysteresis parameters has been found.

3.4. Discussion

Let us start from the correlation between the fluorination degree and conductivity of graphene flakes. As is demonstrated in Feng *et al.*'s review,[40] typical methods of preparing fluorinated graphite or graphene are based on the fluorination in a fluorine containing atmosphere, solutions or plasma treatment, and the F/C ratios and the C–F bonds (covalent, semi-ionic or ionic) usually depend on the fluorination conditions including the pressure, temperature and treatment time. For instance, in the case of plasma SF6 modification of the graphene monolayer with a fluorination degree $\sim$25%, only a weak decrease in the conductivity ($\sim$30%) was observed.[41] Moreover, plasma fluorination

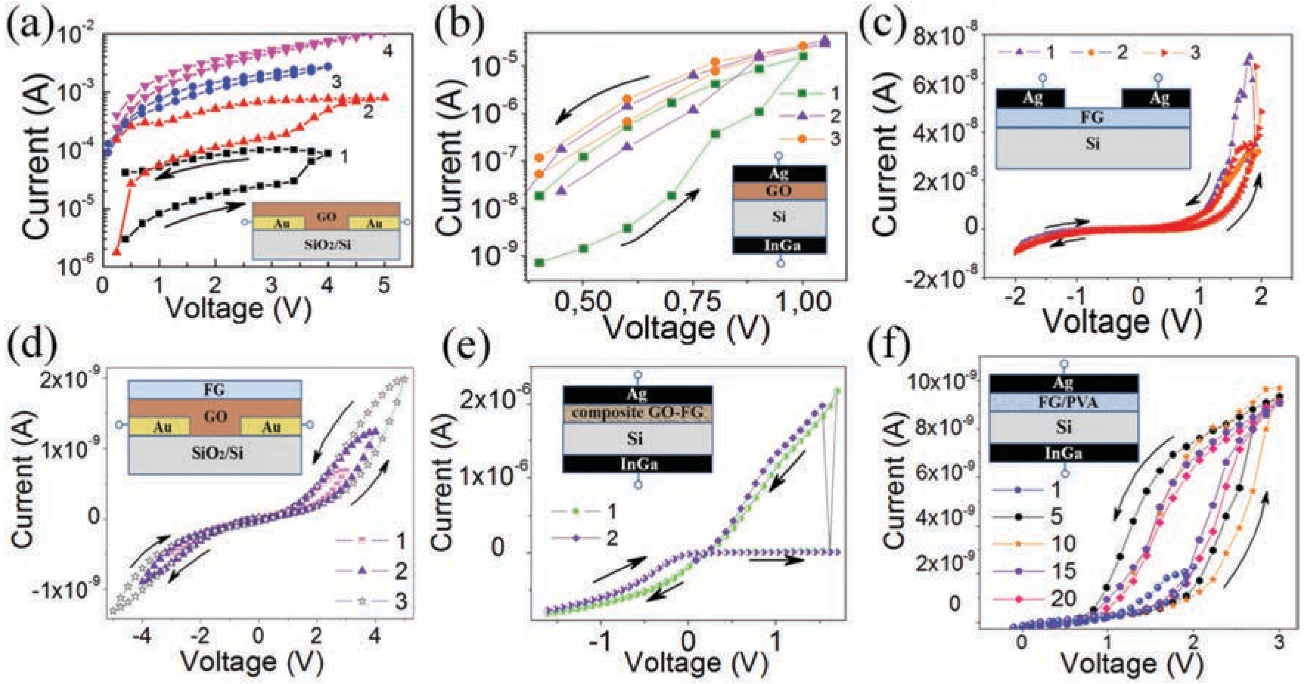

Fig. 8 Current–voltage characteristics of the film structures, insets present the details of the used structures: (a) for the lateral GO_{print} structure with a film thickness of 25–30 nm and a 6 μm distance between contacts; (b) for the vertical GO_{print} structure with a film thickness of 90–110 nm; (c) for the lateral FG_{drop} structure with a film thickness of 25–30 nm; (d) for the lateral FG/GO_{drop} structure with a thickness of 120 nm, the maximum voltage sweep is varied in these measurements; (e) for the vertical structure with a composite $GO–FG_{drop}$ film of 80 nm thickness; and (f) for the vertical FG/PVA_{print} structure. The numbers on the figures designate cycles of the repeated curve recording.

of monolayer graphene yields the formation of polyenes in partially fluorinated graphene ($F/C < 0.25$) opening a transport gap of ~25 meV.[42] So, the partial fluorination degree of graphene ≤25% with different structure and properties of the films is possible. In our case, the fluorination degree can be varied up to ~60%, and the transition to the insulated state occurs at a fluorination degree ~20–25%.[16] This observation is correlated with the theoretical prediction of Wai.[43] High transparency of the suspension and films in visible and near infrared ranges demonstrates the possibility of a strong tuning of the FG properties (opening of large bang gap) after a relatively weak fluorination degree.

Fluorination of graphene oxide or exfoliation of fluorinated graphite leads as a rule to the formation of fluorinated graphene oxide.[25,26,44] In our case, the oxidation degree is negligible. This statement is supported by XPS data and the results of the Raman spectroscopy and the study of thermal stability of FG films (up to 450 °C).[15,16]

Before considering the properties of double-layered films it is necessary to note that the printing technology allows us to completely avoid the mixing of layers by drying the previous layer before the next pass of the printer was performed. Drying is suggested to lead only to the redistribution of FG flakes on the surface. This suggestion is based on the fact that after the printing of FG layers the surface roughness is decreased (from 8.1 for the GO films to 5.7 nm for the FG/GO films).

It is useful to highlight the properties of the two-layer FG/GO and composite GO–FG films that are promising and important for applications. Moreover, it was found that the properties of the films do not depend on the method of the synthesis on the surface of the silicon substrates (by applying drops or 2D printing):

(a) The FG suspension used in the present study for improvement of GO films demonstrates attractive properties such as a high affinity for GO materials (including hydrophilic FG flakes) and possibility of fabricating a FG suspension with very small (~20 nm in lateral size) and thin (0.4–2 nm) flakes. These properties make GO and FG suspensions related to each other, and allow using the FG suspension to reduce the roughness and eliminate structural defects of the GO films. Structural defects in GO films are connected with edges of the stacked and interlinked flakes in the films. In some cases, a coupling of the edge related defects forms a single defect complex which passes through the films. It resulted in the strong changes in the properties of the GO films, both in cases of a very small thickness (a few nanometers) of FG films covering the GO films and the addition of a low FG concentration to the GO suspension. The fact of the structural defect elimination in two-layer FG/GO films is supported by a strong decrease in the FG/GO surface roughness in comparison to GO.

It is worth mentioning here that decoration of graphite or graphene by metal or polymer particles is a well known effect, and the points where nanoparticles find a lodgment are generally correlated with defects or edges.[45,46] The sensor properties of graphene are also based on similar defect related bases. Defectless monocrystalline graphene is known to be unable to accept the gas molecules or other substances on their surface.[47]

(b) Currents through the two-layer FG/GO structures are lower than through the separate FG and GO films, Fig. 6a–c. So, applying an insignificant fluorinated graphene layer (∼2–3 nm) on the surface of the GO films increases the resistance of the printed structure by 2–3 orders of magnitude. Low values of currents through the two-layer films allow using them as insulating layers for practical applications. This effect is supposed to result from blocking of graphene oxide conductivity by small FG flakes. A significant decrease in the FG/GO film roughness (from 8.1 nm for GO films to 5.7 nm for FG/GO films) suggests the formation of FG few layers on the structural defects of GO films (a local insulating island with a thickness exceeding the average FG film thickness).

(c) Another property of the two-layer FG/GO films important and relevant for their application is their thermostability, namely, a weak change in resistance during annealing regardless of the film thickness that is due to the low degree of GO recovery under these conditions. It is well known that the resistivity of GO films significantly changes at an annealing temperature of 100 °C and higher.[18] Whereas, the FG films are stable up to 450 °C.[15] FG coating suppresses the oxygen migration and removal from the GO layer, especially in the ''weakest'' points near the defects the most intensely decorated by FG flakes.

(d) Addition of a small amount of the FG suspension (∼10–20%) to the GO suspension allows reducing the amount of built-in (fixed) charge and the charge of the surface states in the composite films. The effect is presumably based on good FG and GO affinity and the smaller flake size of the FG suspension, resulting in the films with a denser structure. The standard values of built-in fixed charge density in the widely used Al_2O_3 films are in the range 10^{12}–10^{13} cm^{-2},[48] in HfO_2 they vary within 10^{11}–10^{12} cm^{-2},[49] and in the $Si/SiO_2/Al_2O_3$ structures they range within 10^{11}–10^{13} cm^{-2}.[50] In the composite GO–FG films studied in this work the density of the built-in charge was minimum $(0.4–1) \times 10^{10}$ cm^{-2}, and for the two-layer FG/GO films it was slightly higher $(0.3–1.4) \times 10^{11}$ cm^{-2} (Table 1). However, in general, the values of charges in the films and on heterointerfaces were quite low, including single-layer FG and GO films. Thus, this parameter of the obtained films makes them highly promising for applications as an insulating and protected material in a wide spectrum of devices.

(e) The effective dielectric constant of the films varies in the range from 1.1 to 4.3, depending on the structure and composition (Table 1). The value of the effective dielectric constant of the composite GO–FG films and two-layer FG/GO films depends on the ratio of the film component GO (ε = 4.3)[33,34] and FG (ε = 1.1).[35] Thus, the effective permittivity calculation for two-layer films based on their parameters (layer thickness) well coincides with the experimentally determined values. The possibility to change the dielectric constant of the films by changing their composition is important for applications.

(f) The classical bipolar resistive effect similar to the one discussed in ref. 51 was observed in almost all films based on graphene compounds. Fluorinated graphene is the most stable graphene derivative. So, the synthesis of the FG based composites allows us to observe the effect of resistance switching. The most stable effects were found in two-layer films. FG/GO films show stable but relatively small resistance switching (∼3 times). For practical applications the reduction of resistance at least on one order of magnitude is required. Some variations in the film thickness (an increase in the thickness of both layers) do not lead to an increase in the resistance switching effect. In general, the further search for more perspective structure design is necessary. The FG/PVA films demonstrated the strongest and the most stable unipolar resistive effect. In this case, one order of the resistance switching is provided. The origin of the resistive effect in our films is unknown and requires further investigations.

Combination of the properties such as low conductivity of layers, ultra-low values of charges in the film and on the interface with a semiconductor, the variation of permittivity and possible deposition of suspensions on flexible substrates makes the two-layer and composite films promising for use as dielectric layers (substrates for graphene, gate dielectrics, interlayer insulators, protective coatings, *etc.*) in the heterostructures, transistors, logic elements based on graphene, *i.e.* for graphene, flexible and printed electronics. The problem of graphene adhesion to graphene oxide and/or fluorinated graphene is solved by treating in isopropyl alcohol or creating special adhesive coatings. The detected resistive effect allows thinking about the prospects of using these films to develop materials for memristors.

GO films were tested as gate dielectrics in field effect transistor structures.[36,38,52,53] The breakdown electric field of graphene oxide was found to be comparable to SiO_2, typically $\sim(1–3) \times 10^6$ V cm^{-1}, while the GO dielectric constant was slightly higher than that for SiO_2, $\kappa \approx 4.3$. The carrier mobility in field effect transistors was found to be equal to ∼300–700 cm^2 V^{-1} s^{-1}. The maximum transconductance of 0.42 mS and the intrinsic cut off frequency of 117 GHz were achieved.[53] The main advantage of the GO films is their excellent flexibility. Generally, in all cases the relatively high leakage current was mentioned: from ∼20 A cm^{-2} for 4 nm GO[53] to 17 mA cm^{-2} for 100 nm thick GO films.[36] According to our results, the relatively large leakage current and a strong limitation on enhanced temperature (even under the current flow) may be improved by combining GO and FG. The leakage current found in our films was lower than 0.1–1 μA and corresponded to a current density of 0.02–0.2 mA cm^{-2} in two layer and composite films.

Especially it is worth emphasizing that the possibility of using 2D printed technologies allows creating not only GO but also FG layers, widening the range and perspectives of two-layered film applications.

4. Conclusions

The two-layer and composite films based on graphene oxide and fluorinated graphene have been fabricated and studied. Deposition of fluorinated graphene on the graphene oxide films reduces the current through the structure by the value from 2 to 5 orders of magnitude and makes the structure more resistant to temperature. A decrease in leakage current was found to be due to decoration and elimination of structural defects in the graphene oxide films by small FG flakes. The annealing of the two-layer FG/GO films at temperatures up to 350 °C leads to a decrease in resistance by just an order instead of 3–5 orders of magnitude for the GO films. In the metal–insulator–semiconductor Ag/FG/GO/Si structures it was found that the fixed charge in the FG/GO films and at the interface with silicon is relatively low $(0.3\text{–}2) \times 10^{11}$ cm^{-2}. Creating films from the composite GO–FG suspension with the FG content of 10–20% leads to ultra-low values of charges in the films and at the interface with silicon $(0.4\text{–}1) \times 10^{10}$ cm^{-2}. The values of current through the two-layered and composite films are limited within 0.02–0.2 mA cm^{-2}. The relative dielectric permittivity of these films was measured to range from 1.1. (FG) to 4.3 (GO) depending on their composition, which is also important for applications. The synthesis of two-layer FG/GO films preventing recovery of graphene oxide stabilizes the resistive effect, observed in the GO films. The stable resistive effect with the value of resistance change up to two orders of magnitude was revealed in the composite films of FG-polyvinyl alcohol. All these findings make the two-layer films with the minimal leakage current, the composite GO–FG films with the minimal built-in charge, and the films of FG-polyvinyl alcohol with the maximal and the most stable resistive effect promising for a wide spectrum of applications instead of single GO films. These two-layer and the composite graphene based materials are the most promising materials for creating dielectric layers (gate dielectrics, interlayer insulators, and so on) in devices produced using different methods including 2D printing for graphene and flexible electronics.

Acknowledgements

The authors express their gratitude to Dr S. A. Smagulova Scientific Researcher of Ammosov North-Eastern Federal University for the graphene oxide suspension and V. B. Timofeev, from the same University, for his assistance in the scanning electron microscopy measurements. We are grateful to Dr V. A. Volodin from A. V. Rzhanov Institute of Semiconductor Physics SB RAS for the film transmission measurements. This study was financially supported in part by the Russian Science Foundation (grant no. 15-12-00008).

Notes and references

1 S. Gambhir, R. Jalili, D. L. Officer and G. G. Wallace, *NPG Asia Mater.*, 2015, **7**, e186.

2 Y. Gao, W. Shi, W. Wang, Y. Leng and Y. Zhao, *Ind. Eng. Chem. Res.*, 2014, **53**, 16777–16784.

3 M. Magliulo, M. Y. Mulla, M. Singh, E. Macchia, A. Tiwari, L. Torsi and K. Manoli, *J. Mater. Chem. C*, 2015, **3**, 12347–12363.

4 L. Huang, Y. Huang, J. Liang, X. Wan and Y. Chen, *Nano Res.*, 2011, **4**, 675–684.

5 K. Ojha, O. Anjaneyulu and A. K. Ganguli, *Curr. Sci.*, 2014, **107**, 397.

6 D. J. Finn, M. Lotya, G. Cunningham, R. J. Smith, D. McCloskey, J. F. Donegan and J. N. Coleman, *J. Mater. Chem. C*, 2014, **2**, 925–932.

7 F. Withers, H. Yang, L. Britnell, A. P. Rooney, E. Lewis, A. Felten, C. R. Woods, V. Sanchez Romaguera, T. Georgiou, A. Eckmann, Y. J. Kim, S. G. Yeates, S. J. Haigh, A. K. Geim, K. S. Novoselov and C. Casiraghi, *Nano Lett.*, 2014, **14**, 3987–3992.

8 A. M. Rodrıguez, A. B. Muñoz-García, O. Crescenzi, E. Vázquez and M. Pavone, *Phys. Chem. Chem. Phys.*, 2016, **18**, 22203–22209.

9 P. Singla, M. Riyaz, S. Singhal and N. Goel, *Phys. Chem. Chem. Phys.*, 2016, **18**, 5597–5604.

10 L. Grande, V. T. Chundi, D. Wei, C. Bower, P. Andrew and T. Ryhänen, *Particuology*, 2012, **10**, 1–8.

11 P. T. Yin, S. Shah, M. Chhowalla and K. B. Lee, *Chem. Rev.*, 2015, **115**, 2483–2531.

12 J. Li, M. C. Lemme and M. Östling, *ChemPhysChem*, 2014, **15**, 3427–3434.

13 S. Santra, G. Hu, R. C. T. Howe, A. De Luca, S. Z. Ali, F. Udrea, J. W. Gardner, S. K. Ray, P. K. Guha and T. Hasan, *Sci. Rep.*, 2015, **5**, 17374.

14 S. Lim, B. Kang, D. Kwak, W. H. Lee, J. A. Lim and K. Cho, *J. Phys. Chem.*, 2012, **116**, 7520–7525.

15 N. A. Nebogatikova, I. V. Antonova, V. Ya. Prinz, V. A. Volodin, D. A. Zatsepin, E. Z. Kurmaev, I. S. Zhidkov and S. O. Cholakh, *Nanotechnol. Russ.*, 2014, **9**, 51–59.

16 N. A. Nebogatikova, I. V. Antonova, V. Ya. Prinz, I. I. Kurkina, V. I. Vdovin, G. N. Aleksandrov, V. B. Timofeev, S. A. Smagulova, E. R. Zakirova and V. G. Keslera, *Phys. Chem. Chem. Phys.*, 2015, **17**, 13257–13266.

17 I. I. Kurkina, I. V. Antonova, N. A. Nebogatikova, A. N. Kapitonov and S. A. Smagulova, *J. Phys. D: Appl. Phys.*, 2016, **49**, 095303.

18 G. N. Alexandrov, S. A. Smagulova, A. N. Kapitonov, F. D. Vasil'eva, I. I. Kurkina, P. V. Vinokurov, V. B. Timofeev and I. V. Antonova, *Nanotechnol. Russ.*, 2014, **9**, 363–368.

19 N. A. Nebogatikova, I. V. Antonova, I. I. Kurkina, R. A. Soots, V. I. Vdovin, V. B. Timofeev, S. A. Smagulova and V. YaPrinz, *Nanotechnology*, 2016, **27**, 205601.

20 K. I. Ho, C. Huang, J. Liao, W. Zhang, L. Li, C. Lai and C. Su, *Sci. Rep.*, 2014, **4**, 5893.

21 R. R. Nair, W. C. Ren, R. Jalil, I. Riaz, V. G. Kravets, L. Britnell, P. Blake, F. Schedin, A. S. Mayorov, S. Yuan, M. I. Katsnelson, H. M. Cheng, W. Strupinski, L. G. Bulusheva, A. V. Okotrub, I. V. Grigorieva, A. N. Grigorenko, K. S. Novoselov and A. K. Geim, *Small*, 2010, **6**, 2877–2884.

22 Y. Wang, W. C. Lee, K. K. Manga, P. K. Ang, J. Lu, Y. P. Liu, C. T. Lim and K. P. Loh, *Adv. Mater.*, 2012, **31**, 4285–4290.

23 X. Wang, Y. Dai, J. Gao, J. Huang, B. Li, C. Fan, J. Yang and X. Liu, *ACS Appl. Mater. Interfaces*, 2013, **5**, 8294–8299.

24 C. Sun, Y. Feng, Y. Li, C. Qin, Q. Zhang and W. Feng, *Nanoscale*, 2014, **6**, 2634–2641.

25 Z. Wang, J. Wang, Z. Li, P. Gong, X. Liu, L. Zhang, J. Ren, H. Wang and S. Yang, *Carbon*, 2012, **50**, 5403–5410.

26 M. Bruna, B. Massesi, C. Cassiago, A. Battiato, E. Vittone, G. Speranza and S. Borini, *J. Mater. Chem.*, 2011, **21**, 18730–18737.

27 Y. V. Lavskaya, L. G. Bulusheva, A. V. Okotrub, N. F. Yudanova, D. V. Vyalikh and A. Fonseca, *Carbon*, 2009, **47**, 1629–1636.

28 I. V. Antonova, I. A. Kotin, V. I. Popov, F. D. Vasilev, A. N. Kapitonov and S. A. Smagulova, *J. Semicond.*, 2016, **50**, 1065–1073.

29 S. Stankovich, D. A. Dikin, G. H. B. Dommett, K. M. Kohlhaas, E. J. Zimney, E. A. Stach, R. D. Piner, S. T. Nguyen and R. S. Ruoff, *Nature*, 2006, **442**, 282–286.

30 R. Ramasubramaniam, J. Chen and H. Liu, *Appl. Phys. Lett.*, 2003, **83**, 2928–2930.

31 P. Fan, L. Wang, J. Yang, F. Chen and M. Zhong, *J. Nanotechnol.*, 2012, **23**, 365702.

32 I. Mutlay and L. B. Tudoran, *Fullerenes, Nanotubes, Carbon Nanostruct.*, 2014, **22**, 413–433.

33 M. A. Ribas, A. K. Singh, P. B. Sorokin and B. I. Yakobson, *Nano Res.*, 2011, **4**, 143–152.

34 J. Li and J.-K. Kim, *Compos. Sci. Technol.*, 2007, **67**, 2114.

35 A. Dani and A. A. Ogale, *Compos. Sci. Technol.*, 1996, **56**, 911.

36 B. Standley, A. Mendez, E. Schmidgall and M. Bockrath, *Nano Lett.*, 2012, **12**, 1165–1169.

37 X. Huang, C. Zhi, P. Jiang, D. Golberg, Y. Bando and T. Tanaka, *J. Nanotechnol.*, 2012, **23**, 455705.

38 H. Y. Jeong, J. Y. Kim, J. W. Kim, J. O. Hwang, J.-E. Kim, J. Y. Lee, T. H. Yoon, B. J. Cho, S. O. Kim, R. S. Ruoff and S.-Y. Choi, *Nano Lett.*, 2010, **10**, 4381–4386.

39 C. C. Lin, H. Y. Wu, N. C. Lin and C. H. Lin, *Jpn. J. Appl. Phys.*, 2014, **53**, 05FD03.

40 W. Feng, P. Long, Y. Feng and Y. Li, *Adv. Sci.*, 2016, **3**, 1500413.

41 G. Bruno, G. V. Bianco, M. M. Giangregorio, M. Losurdoa and P. Capezzuto, *PhysChemComm*, 2014, **16**, 13948–13955.

42 G. Bruno, G. V. Bianco, M. M. Giangregorio, M. Losurdo and P. Capezzuto, *Phys. Chem. Chem. Phys.*, 2014, **16**, 13948–13955.

43 W. Wei and T. Jacob, *Phys. Rev. B: Condens. Matter Mater. Phys.*, 2013, **87**, 115431.

44 P. Gong, J. Wang, K. Hou, Z. Yang, Z. Wang, Z. Liu, X. Han and S. Yang, *Carbon*, 2017, **112**, 63–71.

45 Y. Yang, J. Wang, J. Zhang, J. Liu, X. Yang and H. Zhao, *Langmuir*, 2009, **25**, 11808–11814.

46 K. Liu, L. Liu, L. Luo and D. Jia, *J. Mater. Chem.*, 2012, **22**, 20342.

47 A. C. Ferrari, F. Bonaccorso, V. Fal'ko, K. S. Novoselov, S. Roche, P. Boggild, S. Borini, F. H. L. Koppens, V. Palermo, N. Pugno, J. A. Garrido, R. Sordan, A. Bianco, L. Ballerini, M. Prato, E. Lidorikis, J. Kivioja, C. Marinelli, T. Ryhänen, A. Morpurgo, J. N. Coleman, V. Nicolosi, L. Colombo, A. Fert, M. Garcia-Hernandez, A. Bachtold, G. F. Schneider, F. Guinea, C. Dekker, M. Barbone, Z. Sun, C. Galiotis, A. N. Grigorenko, G. Konstantatos, A. Kis, M. Katsnelson, L. Vandersypen, A. Loiseau, V. Morandi, D. Neumaier, E. Treossi, V. Pellegrini, M. Polini, A. Tredicucci, G. M. Williams, B. H. Hong, J.-H. Ahn, J. M. Kim, H. Zirath, B. J. van Wees, H. van der Zant, L. Occhipinti, A. D. Matteo, I. A. Kinloch, T. Seyller, E. Quesnel, X. Feng, K. Teo, N. Rupesinghe, P. Hakonen, S. R. T. Neil, Q. Tannock, T. Löfwander and J. Kinaret, *Nanoscale*, 2015, **7**, 4587–5062.

48 B. Hoex, J. J. H. Gielis, M. C. M. Van de Sanden and W. M. M. Kessels, *J. Appl. Phys.*, 2008, **104**, 113703.

49 R. Garg, N. A. Chowdhury, M. Bhaskaran, P. K. Swain and D. Misra, *J. Electrochem. Soc.*, 2004, **151**, F215–F219.

50 N. M. Terlinden, G. Dingemans, V. Vandalon, R. H. E. C. Bosch and W. M. M. Kessels, *J. Appl. Phys.*, 2014, **115**, 033708.

51 R. Waser and M. Aono, *Nat. Mater.*, 2007, **6**, 833–840.

52 S.-K. Lee, H. Y. Jang, S. Jang, E. Choi, B. H. Hong, J. Lee, S. Park and J.-H. Ahn, *Nano Lett.*, 2012, **12**, 3472–3476.

53 M. U. Jewel, T. A. Siddiquee and M. R. Islam, Electrical Information and Communication Technology (EICT) International Conference. IEEE.,2013, 1–5.